AIAA 82-4151

Wind-Tunnel Wall Interference Corrections for Three-Dimensional Flows

M. H. Rizk* and M. G. Smithmeyer†
Flow Research Company, Kent, Wash.

A procedure for the evaluation of wall interference corrections for three-dimensional aircraft configurations is presented. The Mach number and angle-of-attack corrections are obtained by numerically solving the Laplace equation in a parallelepiped with boundary conditions supplied mainly from experimental pressure measurements. A portion of these measurements and other wind-tunnel data required by the procedure may be replaced by theoretical estimates if not available from experiments. The accuracy of the correction results will then depend on the accuracy of these estimates. The correction procedure is applied to an isolated wing and to a wing-tail configuration in a solid-wall wind tunnel. It is found that neglecting twist and camber corrections for the wing effectively increases the tail angle-of-attack correction. Two different Mach number corrections can be calculated for the wing and tail. However, since only one Mach number correction is allowed for both the wing and the tail, and since the wing surface area is larger than the tail surface area, the final correction tends to be closer to the required wing correction. This is a source of error for the tail results.

Nomenclature

B.L. = body length
k = ratio of specific heats
L = spanwise lift distribution
M = Mach number
q = velocity
s = source strength
S' = rate of change of the cross-sectional area distribution along the body
S_M = model surface
S_w = wing planform
S.C. = section chord
t = wing thickness
u,v,w = velocity components in the x,y,z directions
W.S. = wing span
x,y,z = Cartesian coordinate system
X_w = x coordinate relative to wing leading edge
Y_w = y/wing semispan
α = angle of attack
γ = bound vorticity strength = difference between u on wing top and bottom surfaces
ϕ = perturbation velocity potential

Subscripts

c = body axis
w = wing
∞ = undisturbed condition

Superscripts

b = body
c = correction
cc = camber correction
ce = local correction value
F = free air
l = lift
Mc = Mach number correction
t = thickness
tc = twist correction
T = tunnel
w = wing
αc = angle-of-attack correction
τ = tail

Received June 15, 1981; revision received Oct. 6, 1981.

*Senior Research Scientist. Member AIAA.
†Senior Research Scientist.

Introduction

As part of a broader program of looking at wall interference correction methods for transonic wind tunnels, a classical correction method adapted to the use of measured wall boundary conditions has been developed for three-dimensional flows. The classical methods for subsonic flows, as first applied to closed or open tunnels and then extended to ventilated wind tunnels, have been summarized by Garner et al.[1] The general characteristics of the classical method are as follows. The flow field satisfies the linear Prandtl-Glauert (P.G.) equation. The complicated flow near the ventilated tunnel wall is represented by a linear homogeneous boundary condition with two arbitrary numerical coefficients, one to describe the porosity effect and the other the slot effect. The concept of a wall interference flow is introduced. An analytic free-air solution is derived, using sources and/or doublets and vortices to represent the model. The wall interference flow is then defined as that flow which, when added to the free-air solution, satisfies the wall boundary conditions. This interference flow can be interpreted as providing corrections to the tunnel stream direction and speed. The interference flow may also introduce streamline curvature and a streamwise pressure gradient, providing corrections to pitching moment and drag.

The basic classical approach as applied to two-dimensional flows has been examined and modified by various investigators. Mokry et al.[2] measured pressures near the walls to examine the validity of the classical approach for high-subsonic flows and to determine porosity factors. Kemp[3,4] proposed using measured pressure distributions rather than the homogeneous wall boundary conditions and calculated examples of his method at both subsonic and transonic speeds. Murman[5] used measured pressure distributions for a boundary condition near the wall but departed from the classical approach in finding the "corrected" Mach number M and angle of attack α. He calculated the flow about the "given" airfoil in a freestream, optimizing M and α to obtain the least error in matching the calculated model pressures to the measured model pressures. Mokry and Ohman[6] retain the classical approach in finding the corrected M and α, but use measured pressure distributions near the wall (and one flow direction measurement) as boundary conditions for their wall

interference flow. This interference flow is calculated numerically with a fast Fourier transform technique.

The present paper describes a wall interference correction method which is essentially an extension of the two-dimensional Mokry-Ohman method to three-dimensional flows. The basic assumption is that the flow in the tunnel in the region of the walls satisfies the linear P.G. equation. Furthermore, it is assumed that, in the neighborhood of the walls but with the walls removed, the (unknown) free-air solution also satisfies the P.G. equation. This free-air solution is approximated by analytic solutions of the P.G. equation using source and vortex singularities at the model location. These singularities provide the measured lift and specified spanwise distributions of lift and thickness at the tunnel value of M. The wall interference flow is then that flow which, when added to the analytic free-air solution, satisfies the measured pressure near the wall. This fictitious interference flow is determined only from boundary conditions near the tunnel walls and conditions at end planes upstream and downstream of the model location. For this fictitious flow, the model is not present and the flowfield is smooth and well-behaved and can be assumed to satisfy the P.G. equation throughout the tunnel domain. The solution is obtained numerically (after a P.G. transformation) using a fast three-dimensional Laplace solver. Details of the procedure, described in terms of a "correction flow" which is the negative of the wall interference flow, are developed below. Examples of the type of information provided by the procedure are given for a solid-wall tunnel.

This wall correction method may provide an adequately corrected value of α even at transonic speeds. It has been observed for two-dimensional flows (see, e.g., Refs. 5, 7, and 8) that linear theory corrections to α are adequate well into transonic speeds. Furthermore, Chan[8,9] has shown analytically, by expansion of the transonic small-disturbance equations, that the angle-of-attack correction to first order in wing chord/tunnel height can be calculated from the linear compressible flow equation.

The wall-corrected value of M obtained by this "modified classical" method is not expected to be adequate at transonic speeds (although for three-dimensional flows the correction should be smaller than for two-dimensional flows because of reduced blockage). However, this value of M could make a good starting value for some more accurate iterative process based on transonic equations.

Formulation

The procedure for correcting three-dimensional wind-tunnel data follows closely that used by Mokry and Ohman[6] for correcting the two-dimensional problem. A model tested in a wind tunnel (see Fig. 1), with a freestream Mach number M_∞^T and an angle of attack α^T, develops a spanwise lift distribution $L^T(y)$. The wind-tunnel correction procedure seeks to find the free-air angle of attack α^F which nearly produces the lift distribution $L^T(y)$ for the model in free air with an undisturbed Mach number M_∞^T. The angle-of-attack correction α^c is then given by

$$\alpha^c = \alpha^F - \alpha^T$$

Let q^T be the velocity of the wind-tunnel flow, and let q^F be the corresponding free-air velocity for the flow with Mach number M_∞^T, which produces the same lift distribution for the model as in the tunnel case. The velocity of the correction flow q^c is then given by

$$q^c = q^F - q^T$$

where all velocities have been normalized by the undisturbed flow speed. In order to find the angle-of-attack and Mach number corrections, it is necessary to find the solution to the correction flow. A boundary-value problem is formulated with boundary conditions applied on the boundaries of a rectangular parallelepiped, whose sides are close to the tunnel walls but outside the boundary-layer region and whose end planes are taken as far upstream and downstream from the model location as possible (see Fig. 1). The rectangular parallelepiped is defined by

$$x_a \le x \le x_b; \qquad y_a \le y \le y_b; \qquad z_a \le z \le z_b$$

Governing Equations

The correction flow velocity q^c is expressed in terms of a potential function ϕ^c as follows:

$$q^c = (u^c, v^c, w^c) = \nabla \phi^c \tag{1}$$

where ϕ^c is governed by the equation

$$\beta^2 \phi^c_{xx} + \phi^c_{yy} + \phi^c_{zz} = 0 \tag{2}$$

$$\beta^2 = 1 - (M_\infty^T)^2$$

and the use of independent variables as subscripts denotes differentiation.

Taking the x derivative of Eq. (2) leads to the equation

$$\beta^2 u^c_{xx} + u^c_{yy} + u^c_{zz} = 0 \tag{3a}$$

This equation, in addition to the irrotationality conditions

$$v^c_x = u^c_y \tag{3b}$$

and

$$w^c_x = u^c_z \tag{3c}$$

composes a system of equations for the velocity components.

Boundary Conditions

Dirichlet boundary conditions for u^c are specified from the relation

$$u^c = u^F - u^T \tag{4}$$

where u^T is determined from wind-tunnel measurements, while u^F is determined from theoretical considerations, as described below. Measurements of u^T may be difficult to make at the end planes of the parallelepiped. In this case some estimate of u^T must be done there. In Ref. 6, a linear interpolation provided such an estimate. This implies that

$$u^T_{xx} = 0$$

which is a reasonable assumption provided the end planes are sufficiently far downstream and upstream of the model location. In the three-dimensional problem, making the same assumption leads to the equation

$$u^T_{yy} + u^T_{zz} = 0 \tag{5}$$

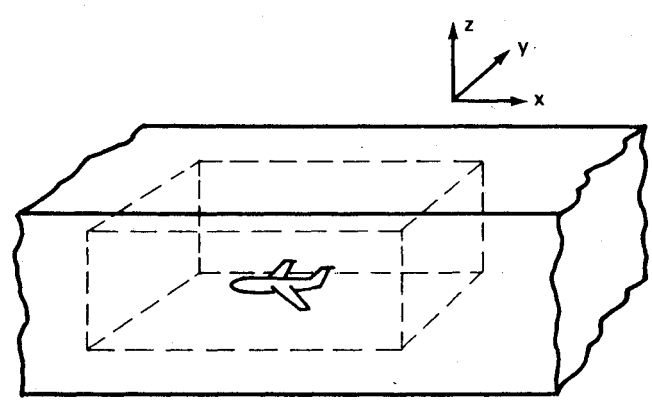

Fig. 1 Geometrical configuration.

After solving Eq. (3a), Eqs. (3b) and (3c) may be viewed as ordinary differential equations with x being the independent variable. The y velocity component v^c is not required for the correction procedure; however, w^c is required at specific points. In order to evaluate $w^c(x,y,z)$, it is necessary to specify $w^c(x_0,y,z)$ where x_0 is arbitrary and is chosen here to coincide with the x coordinate of the upstream boundary of the parallelepiped x_a. The initial condition necessary for determining a unique solution of Eq. (3c) is defined by

$$w^c(x_a,y,z) = w^F(x_a,y,z) - w^T(x_a,y,z) \tag{6}$$

where w^T is measured and w^F is estimated from theoretical considerations described below.

The application of the boundary condition [Eq. (4)] and the initial condition [Eq. (6)] requires an estimate for the free-air flow solutions u^F and w^F on the parallelepiped boundaries in addition to the measured data. In general, a numerical solution of the flow governing equation is required to obtain the flow solution at the parallelepiped boundaries. However, under certain assumptions, simple solutions which do not require the numerical solution of the linear P.G. equation are obtainable. The assumptions are made that the body is slender and the wing and tail are thin. The perturbation potential ϕ is expressed as

$$\phi = \phi^b + \phi^{t,w} + \phi^{l,w} + \phi^{t,\tau} + \phi^{l,\tau}$$

where ϕ^b is the perturbation potential function due to the body, $\phi^{t,w}$ and $\phi^{l,w}$ are the perturbation potential functions due to the wing thickness and the wing lift, respectively, while $\phi^{t,\tau}$ and $\phi^{l,\tau}$ are the corresponding potential functions due to the tail.

At the parallelepiped boundaries, the linearized, small-perturbation potential function ϕ^b is given by[10]

$$\phi^b(x,y,z;y_c,z_c) = -\frac{1}{4\pi}\int_{\text{B.L.}} \frac{S'(x_l)}{R_b(x,y,z;x_l,y_c,z_c)}\,dx_l \tag{7}$$

where

$$R_b(x,y,z;x_l,y_c,z_c) = \sqrt{(x-x_l)^2+\beta^2[(y-y_c)^2+(z-z_c)^2]}$$

The linearized, small-perturbation potential function due to the wing thickness is[10]

$$\phi^{t,w}(x,y,z;z_w) = -\frac{1}{4\pi}\int_{S_w}\int \frac{t_x(x_l,y_l)}{R_b(x,y,z;x_l,y_l,z_w)}\,dx_l\,dy_l \tag{8}$$

and the linearized, small-perturbation potential function due to the wing lift is[10]

$$\phi^{l,w}(x,y,z;z_w) = \frac{1}{4\pi}\int_{S_w}\int \frac{(z-z_w)\gamma(x_l,y_l)}{(y-y_l)^2+(z-z_w)^2} \times\left(1+\frac{x-x_l}{R_b(x,y,z;x_l,y_l,z_w)}\right)dx_l\,dy_l \tag{9}$$

Expressions similar to Eqs. (8) and (9) may be written for the potential functions $\phi^{t,\tau}$ and $\phi^{l,\tau}$. Simplified expressions for the potential functions $\phi^{t,w}$ and $\phi^{l,w}$ are derived in the Appendix.

To evaluate the velocity components u^F and w^F on the boundaries, the relation

$$(u^F-1, w^F) = \left(\frac{\partial}{\partial x}, \frac{\partial}{\partial z}\right)(\phi^b+\phi^{t,w}+\phi^{l,w}+\phi^{t,\tau}+\phi^{l,\tau})$$

is used.

Angle-of-Attack and Mach Number Corrections

The local angle-of-attack correction at a point (x,y,z_w) on the wing is evaluated by integrating Eq. (3c) with respect to x,

$$\alpha^{ce} = -w^c(x,y,z_w) = -w^c(x_a,y,z_w) - \int_{x_a}^{x} u^c_z\,dx \tag{10}$$

This correction may be expressed as

$$\alpha^{ce}(x,y) = \alpha^c + \alpha^{tc}(y) + \alpha^{cc}(x,y)$$

where $\alpha^{tc}(y)$ is the twist correction and $\alpha^{cc}(x,y)$ the camber correction. The angle-of-attack correction for the wing is evaluated by using the formula

$$\alpha^c = \frac{\int_{\text{W.S.}} [\alpha^c + \alpha^{tc}(y)]\,|L^T(y)|\,dy}{\int_{\text{W.S.}} |L^T(y)|\,dy} \tag{11}$$

where

$$\alpha^c + \alpha^{tc}(y) = \frac{\int_{\text{S.C.}} \alpha^{ce}(x,y)\,dx}{\int_{\text{S.C.}} dx} \tag{12}$$

A similar expression may be written for the tail angle-of-attack correction.

Since it is desirable to have similar geometrical configurations for the wind-tunnel and free-air models, the corrections α^{tc} and α^{cc} may be replaced by an equivalent lift correction $L^{\alpha c}(y)$ where the lift distribution $L^T(y)+L^{\alpha c}(y)$ results from a free-air angle of attack $\alpha^T+\alpha^c$. The corrections α^{tc}, α^{cc}, and $L^{\alpha c(y)}$ are generally higher order corrections which may be neglected.

Since the Mach numbers in the vicinities of the wind-tunnel model (with $\alpha=\alpha^T$, $M_\infty=M_\infty^T$) and the free-air model (with $\alpha=\alpha^F$, $M_\infty=M_\infty^T$) are expected to differ, a Mach number correction M^c_∞, where

$$M^c_\infty = M^F_\infty - M^T_\infty$$

is required. Here M^F_∞ is the free-air Mach number which will produce similar Mach numbers in the vicinity of both the free-air and tunnel models. The Mach number change M^{ce}_∞ due to a small change in velocity $(-u^c,-v^c,-w^c)$ is

$$M^{ce}_\infty = -M^T_\infty u^c\left(1+\frac{k-1}{2}(M^T_\infty)^2\right) \tag{13}$$

where k is the ratio of specific heats. A single Mach number correction is obtained from the relation

$$M^c_\infty = \frac{\int_{S_M}\int M^{ce}_\infty(x,y,z)\,dS}{\int_{S_M} dS} \tag{14}$$

Correcting the free-air Mach number will in turn produce a correction $L^{Mc}(y)$ in the lift distribution, so that the free-air model (with $\alpha=\alpha^F$, $M_\infty=M^F_\infty$) will have a spanwise lift distribution $L^F(y)$,

$$L^F(y) = L^T(y) + L^{Mc}(y)$$

However, the lift correction $L^{Mc}(y)$ is generally a higher order correction which may be neglected.

The procedure presented here evaluates the lowest order wind-tunnel corrections α^c and M^c. It assumes that the higher order corrections L^{Mc} and $L^{\alpha c}$ are small and does not attempt

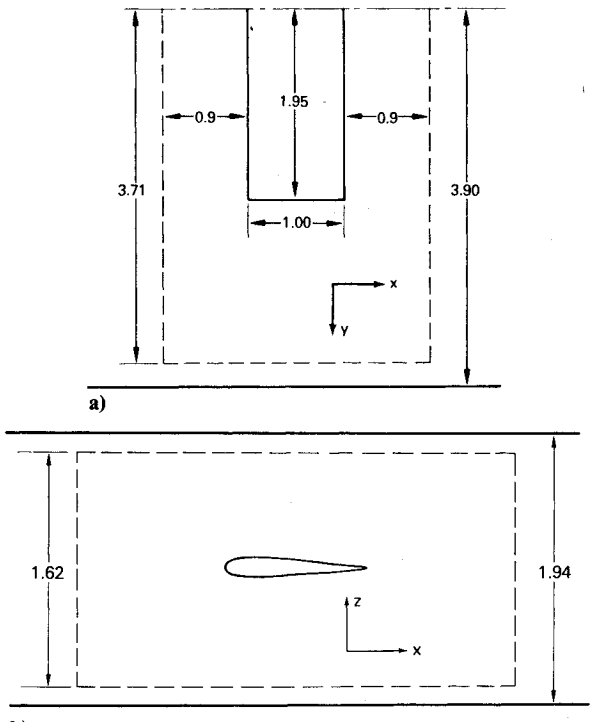

Fig. 2 Wing in tunnel: a) top view and b) side view.

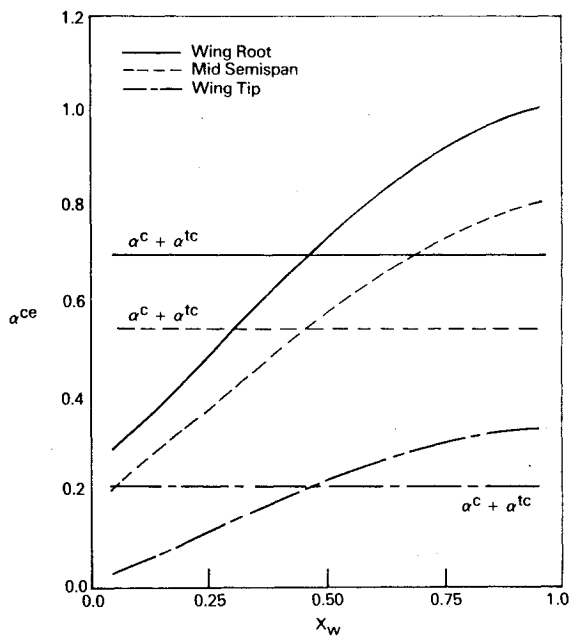

Fig. 3 Local angle-of-attack correction.

to evaluate these lift corrections. However, the procedure provides the necessary information required to evaluate these lift corrections. Since the correction procedure provides the Mach number correction M^c, the spanwise correction in lift distribution L^{Mc} can be directly related to L^Tthrough the use of the Prandtl-Glauert transformation. Moreover, the higher order camber and twist corrections α^{cc} and α^{tc} are evaluated as part of the procedure and may be used, if required, to evaluate $L^{\alpha c}$.

Results and Discussion

The above ideas were used in the development of a computer code which predicts Mach number and angle-of-attack corrections for wind-tunnel models. A computer code for the efficient solution of elliptic partial differential equations[11] is

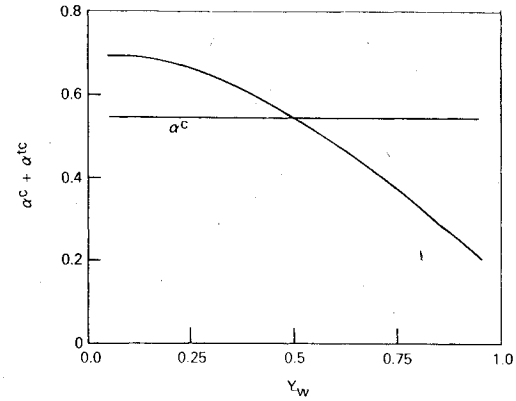

Fig. 4 Angle-of-attack correction along the wing span.

used to solve Eq. (3a). The code uses the fast Fourier transform method in two of the coordinate directions and solves a tridiagonal system of algebraic equations in the third direction. Simpson's rule is used for evaluating the integral in Eq. (10) and the integrals in the free-air expressions for u^F and w^F.

Mach number and angle-of-attack corrections are calculated for a rectangular wing. The geometrical configurations of the wing in the wind tunnel is shown in Fig. 2. The angle of attack in the wind tunnel α^T is chosen to be 3 deg, while the undisturbed wind-tunnel Mach number M_∞^T is taken to be 0.7.

In order to find the Mach number and angle-of-attack corrections, measured data are required on the parallelepiped boundaries. In the following calculations, the measured data are replaced by numerical, finite-difference solutions simulating the flow in a wind tunnel with solid walls. A NACA 0012 airfoil section with the profile $z=f(x)$ is used in the calculations. The boundary conditions at the wing surface is approximated by the small-disturbance condition

$$\phi_z(x,y,z_w) = f_x(x)$$

This approximation creates an error which is equivalent to a source term of strength

$$s = \Delta x \sum_{i=I,N} f_x(x_i)$$

where Δx is the mesh spacing in the x direction and x_i, $i=1,\ldots N$ are the x coordinates of mesh points falling between the wing leading and trailing edges. In order to eliminate this source term the following modified boundary condition is applied

$$\phi_z(x,y,z_w) = f_x(x) - s/\text{chord length}$$

The calculated local angle-of-attack correction α^{ce} along the wing root, midsemispan, and wing tip sections is shown in Fig. 3. The deviation of α^{ce} from the section angle-of-attack correction $\alpha^c + \alpha^{tc}$ indicates the correction in camber. Figure 4 shows the calculated section angle-of-attack correction along the span where $Y_w = y/$wing semispan. The deviation of this correction from α^c indicates the correction in twist. In Fig. 5, local Mach number corrections are shown along the wing root, midsemispan, and wing tip sections. The horizontal line in the figure shows the Mach number correction M^c.

A comparison between the spanwise lift distribution for the wind-tunnel flow ($M_\infty = 0.7$, $\alpha = 3$ deg), the free-air flow at the corrected conditions ($M_\infty = 0.7105$, $\alpha = 3.5482$ deg), and the free-air flow at the uncorrected conditions ($M_\infty = 0.7$, $\alpha = 3$ deg) is given in Fig. 6. The difference between the wind-tunnel spanwise lift distribution and the corrected free-air lift

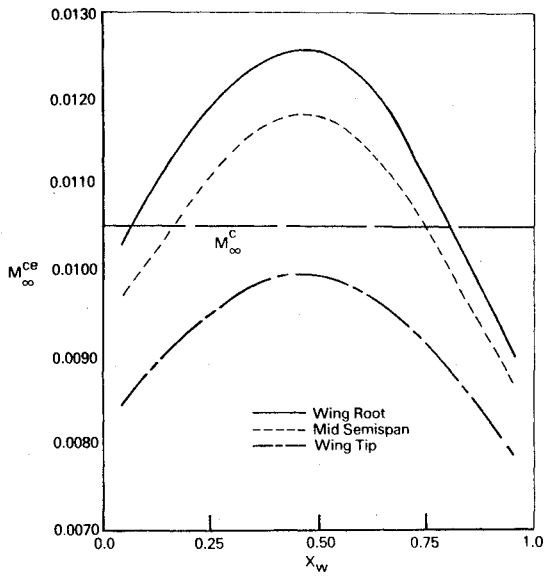

Fig. 5 Local Mach number correction.

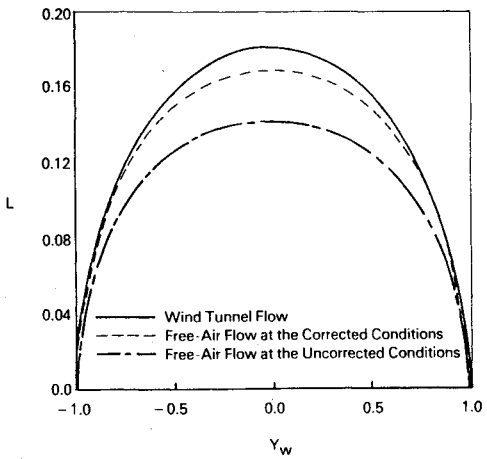

Fig. 6 Spanwise lift distribution.

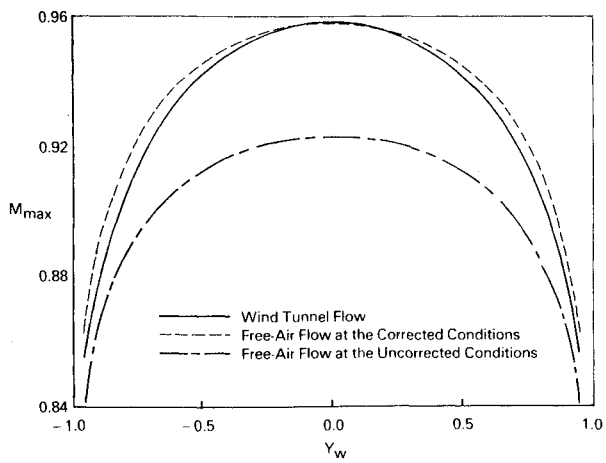

Fig. 7 Maximum Mach number distribution along wing top.

distribution is due to the higher order corrections L^{Mc} and $L^{\alpha c}$. Figures 7 and 8 show the distribution of M_{max} (the maximum Mach number along a chord) along the wing span. Figure 7 indicates that applying the calculated corrections to the free-air problem reduces the maximum Mach number error on the wing's top surface from 0.035 to 0.005. The

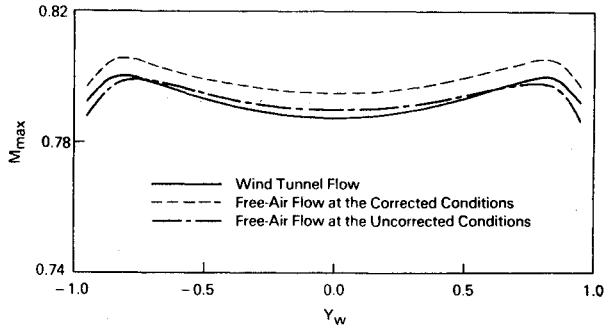

Fig. 8 Maximum Mach number distribution along wing bottom.

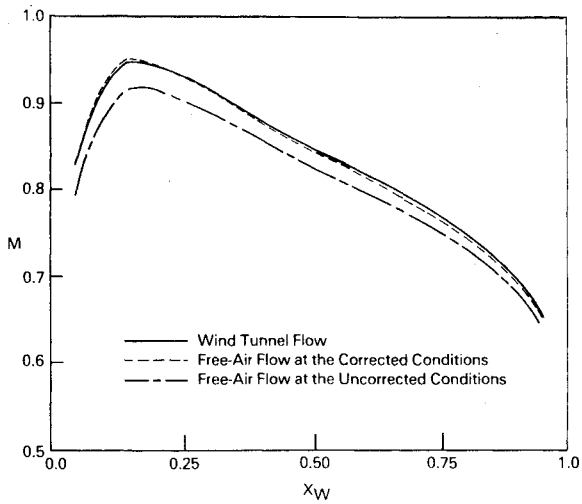

Fig. 9 Mach number distribution on wing top at the midsemispan station.

results for the bottom wing surface shown in Fig. 8 are not as dramatic; however, the maximum Mach number error is of the same order as that for the top surface. Figures 9 and 10 show the Mach number distributions on the wing top and bottom surfaces at the midsemispan station.

The method used here for predicting angle-of-attack and Mach number corrections allows the introduction of a number of approximations which will simplify the correction procedure. Measurements of the streamwise velocity component in the wind tunnel u^T may cause experimental difficulties at the parallelepiped's upstream and downstream end planes. Equation (5) provides an estimate for u^T at the end planes which may be used instead of the measured values. The corrections ($\alpha^c = 0.5133$ deg, $M^c = 0.0106$) which result from using Eq. (5) closely approximate the corrections ($\alpha^c = 0.5482$ deg, $M^c = 0.0105$) found using actual end-plane "measurements." The difference between the two results is expected to decrease as the upstream and downstream end planes are moved further from the model. An estimate for the vertical velocity component w^T at a number of points on the upstream plane of the parallelepiped is required for finding the angle-of-attack correction. Since measurements of w^T on the upstream plane may be difficult, it would be beneficial to use nonmeasured estimates. If the upstream plane is sufficiently far from the tested model, the vertical velocity component is expected to be small and to have a value close to the free-air farfield solution. Setting w^T equal to zero on the upstream plane is found to underestimate the angle-of-attack correction ($\alpha^c = 0.3675$ deg), while setting w^T equal to the free-air farfield solution there is found to overestimate the angle-of-attack correction ($\alpha^c = 0.7714$ deg). As expected, the use of estimated values for w^T instead of the measured values does not affect the Mach number correction ($M^c = 0.0105$). As the upstream boundary is moved further away from the model, these results are expected to approach the results

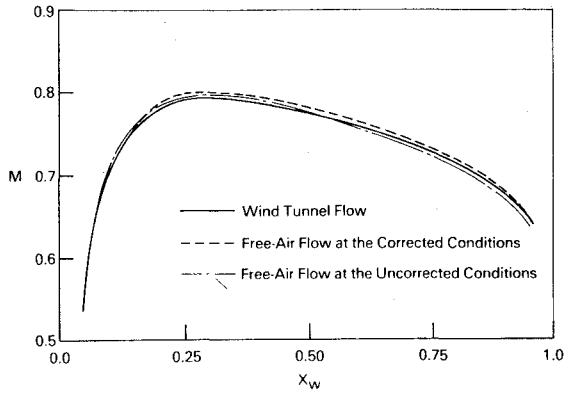

Fig. 10 Mach number distribution on wing bottom at the mid-semispan station.

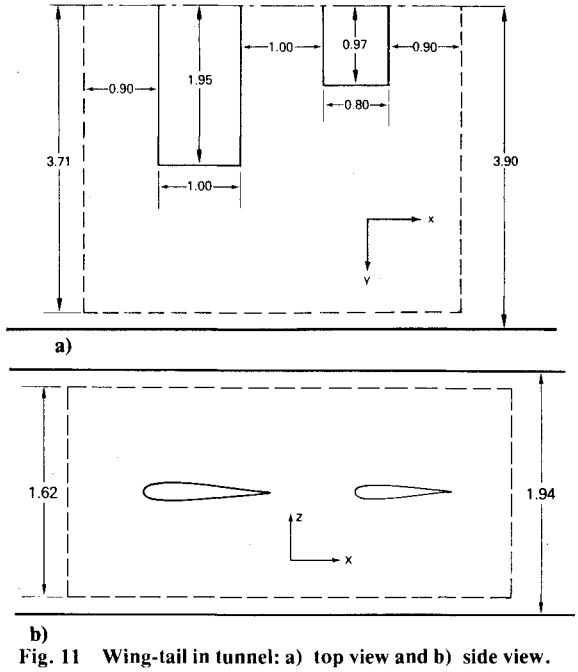

Fig. 11 Wing-tail in tunnel: a) top view and b) side view.

obtained by using measured values for w^T. Setting w^T equal to half the free-air farfield solution on the upstream plane, the correction values ($\alpha^c = 0.5694$ deg, $M^c = 0.0105$) are found to closely approximate the corrections $\alpha^c = 0.5482$ deg, $M^c = 0.0105$. It is not suggested that half the free-air farfield solution is a good value to be used for w^T in general. However, if experimental data are not available, then some theoretical or empirical estimate must be made for these data.

Mach number and angle-of-attack corrections are calculated for a wing-tail configuration shown in Fig. 11. The wing angle of attack is chosen to be 3 deg, while the tail angle of attack is chosen to be 4 deg. The undisturbed wind-tunnel Mach number M_∞^T is taken to be 0.7. Following the correction procedure estimates are made for the Mach number correction ($M^c = 0.0087$), the wing angle-of-attack correction ($\alpha^{c,w} = 0.5266$ deg), and the tail angle-of-attack correction ($\alpha^{c,T} = 1.3405$ deg). A comparison between the spanwise lift distributions for the wind-tunnel flow ($M_\infty = 0.7$, $\alpha^w = 3$ deg, $\alpha^T = 4$ deg), the free-air flow at the corrected conditions ($M_\infty = 0.7087$, $\alpha^w = 3.5266$ deg, $\alpha^T = 5.3405$ deg), and the free-air flow at the uncorrected conditions ($M_\infty = 0.7$, $\alpha^w = 3$ deg, $\alpha^T = 4$ deg) is given in Fig. 12. Neglecting the wing twist correction α^{tc} and the wing camber correction α^{cc} (see Fig. 3) results in an increase in the tail's angle of attack relative to the surrounding flow. This effective increase in the tail's angle of attack results in the overestimated lift distribution along the tail as shown in Fig. 12. The distribution of $M_{\max}$ along the

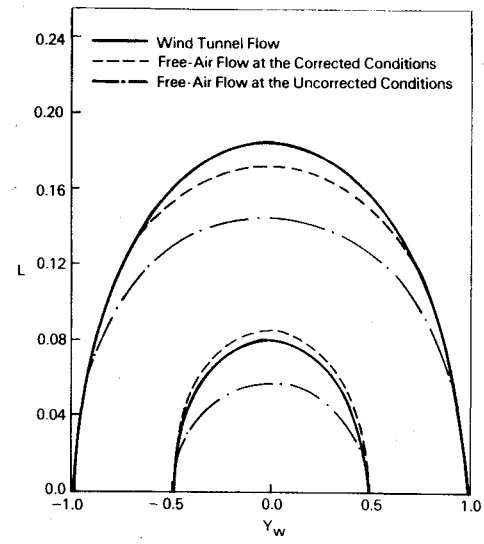

Fig. 12 Spanwise lift distribution for wing and tail.

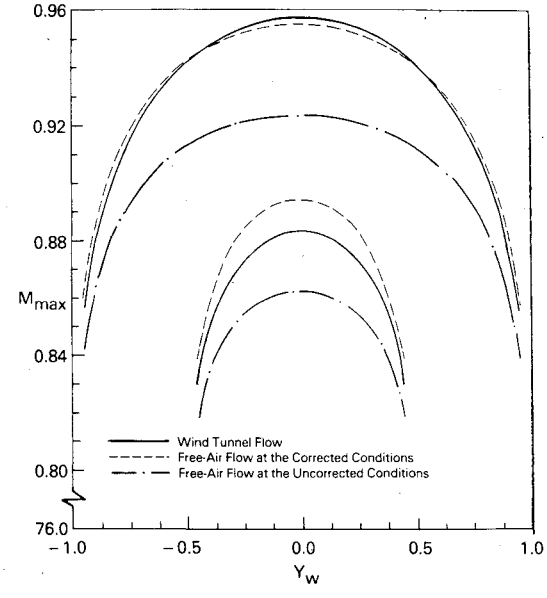

Fig. 13 Maximum Mach number distribution along wing top and tail top.

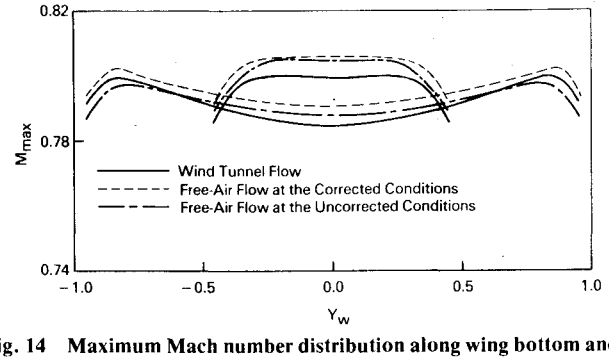

Fig. 14 Maximum Mach number distribution along wing bottom and tail bottom.

wing and tail spans is shown in Figs. 13 and 14. Figure 13 indicates that results along the wing are more accurate than those along the tail. This is due to the fact that the Mach number correction for the wing ($M^{c,w} = 0.0106$) is larger than the Mach number correction for the tail ($M^{c,T} = 0.0040$). However, since only a single Mach number is allowed for both the wing and tail and since the wing's surface area is larger

than that for the tail, Eq. (14) will tend to favor the wing Mach number correction with the result $M^c = 0.0087$.

Conclusions

A method has been developed for the evaluation of wall interference corrections for three-dimensional aircraft configurations. The method is based on linear theory; however, previous studies indicate that the angle-of-attack correction may be used at transonic speeds.

A boundary value problem is formulated for the correction flow from which the Mach number and angle-of-attack corrections are obtained. Experimental data required for the method are the streamwise velocity components on the surface of a rectangular parallelepiped in the wind tunnel, the vertical velocity component at isolated points on the upstream end plane, and the lift distribution along the lifting surfaces. In general, it will not be practical to obtain all of these data experimentally and the replacement of a portion of the data by theoretical estimates may be required. The accuracy of the correction results will then depend on the accuracy of these estimates.

The present correction procedure evaluates the Mach number correction, the wing angle-of-attack correction, and the tail angle-of-attack correction. The higher order twist and camber corrections are also evaluated as part of the procedure; however, the equivalent lift distribution correction due to camber and twist is not evaluated. The higher order lift distribution correction due to the Mach number correction is not evaluated here; however, if necessary this correction may be easily found since it is related to the original lift distribution through a Prandtl-Glauert transformation.

Numerical examples for an isolated wing indicate that the twist and camber effects are small but not negligible for the present solid-wall wind tunnel. These higher order effects are expected to decrease in ventilated wind tunnels and as the wind-tunnel walls are moved away from the model. In the wing-tail configuration the tail angle-of-attack correction is overestimated due to neglecting camber and twist corrections in the wing. Two different Mach number corrections can be calculated for the wing and tail. However, since only one Mach number correction is allowed for both the wing and the tail and since the wing surface area is larger than the tail surface area, the final correction tends to be closer to the required wing correction. This is a source of error for the tail results.

The numerical examples presented here indicate that the correction procedure predicts the Mach number and angle-of-attack corrections with reasonable accuracy. Further calculations are required to determine the conditions under which simple estimates may replace experimental data. The use of real experimental data is also required to evaluate the present approach further.

Appendix

Equation (8) for the potential function $\phi^{l,w}$ is simplified by expanding $1/R_b$ in terms of the binomial series

$$\frac{1}{R_b} = \frac{1}{R}\left[1 - \frac{1}{2}\mu + \frac{3}{8}\mu^2 - \frac{5}{16}\mu^3 + \ldots\right]$$

where

$$\mu = \left[\frac{X_1}{R}\right]\left[\frac{X_1}{R} - 2\frac{X}{R}\right]$$

$$R = \sqrt{X^2 + \beta^2[(y-y_1)^2 + (z-z_w)^2]}$$

$$X = x - x_w(y_1)$$

$$X_1 = x_1 - x_w(y_1)$$

and the function $x_w(y_1)$ is chosen to minimize $|X|$ for all points on the wing in an average sense. If $\mu \ll 1$, only a few terms of the series are sufficient to give a good approximation to $1/R_b$; however, as $\mu \to 1$, an increased number of terms are required. Substituting the expression of $1/R_b$ into Eq. (8), the potential function $\phi^{l,w}$ at points on the parallelepiped boundaries is approximated by

$$\phi^{l,w}(x,y,z;x_w,z_w) = \frac{1}{4\pi}\int_{\text{W.S.}}\left\{\frac{T_0}{R^2}\left(\frac{X}{R}\right) + \frac{T_1}{R^3}\left[3\left(\frac{X}{R}\right)^2 - 1\right] + \frac{3}{2}\frac{T_2}{R^4}\left(\frac{X}{R}\right)\left[5\left(\frac{X}{R}\right)^2 - 3\right] + O(\epsilon^5)\right\}dy_1 \tag{A1}$$

where

$$T_n(y_1) = \int_{\text{S.C.}} t(x_1,y_1)(x_1 - x_w)^n dx_1$$

The parameter ϵ in Eq. (A1) is equal to the maximum value of $|X_1/R|$. The assumption that the wing closes at the trailing edge is made in deriving Eq. (A1). A similar expression to Eq. (A1) may be derived for the perturbation potential function due to the tail thickness, $\phi^{l,\tau}$.

At the boundaries of the parallelepiped, the expression for $\phi^{l,w}$ is approximated by

$$\phi^{l,w}(x,y,z;x_w,z_w) = \frac{\beta^2}{4\pi}\int_{\text{W.S.}}\frac{(z-z_w)}{R}\left\{\frac{\Gamma_0}{R}\left(\frac{1}{1-X/R}\right) - \frac{\Gamma_1}{R^2} - \frac{3}{2}\frac{\Gamma_2}{R^3}\left(\frac{X}{R}\right) - \frac{1}{2}\frac{\Gamma_3}{R^4}\left[5\left(\frac{X}{R}\right)^2 - 1\right] + O(\epsilon^5)\right\}dy_1 \tag{A2}$$

where

$$\Gamma_n(y_1) = \int_{\text{S.C.}} \gamma(x_1,y_1)(x_1 - x_w)^n dx_1$$

Note that $\Gamma_0(y_1)$ is the circulation about the wing section. A similar expression to Eq. (A2) may be derived for the perturbation function due to the tail lift, $\phi^{l,\tau}$.

The lowest order term in Eq. (A1) is $0(\epsilon^2)$, while the lowest order term in Eq. (A2) is $0(\epsilon)$, indicating that away from the wing the flow perturbation due to thickness effects (for a wing which closes at the trailing edge) is of higher order than that due to lift effects.

Acknowledgments

The authors would like to thank E. Murman and M. Cooper for valuable discussions. They also wish to thank the National Center for Atmospheric Research for supplying them with the efficient Laplace solver used in this work. This work was sponsored by NASA Langley under Contract NAS1-16262.

References

[1] Garner, H.C. et al., "Subsonic Wind Tunnel Wall Corrections," AGARDograph 109, Oct. 1966.

[2] Mokry, M., Peake, D.J., and Bowker, A.J., "Wall Interference in Two-Dimensional Supercritical Airfoils Using Wall Pressure Measurements to Determine the Porosity Factors for Tunnel Floor and Ceiling," National Research Council of Canada, Aeronautical Rept. LR-575, Feb. 1974.

[3] Kemp, W.B., Jr., "Toward the Correctable-Interference Transonic Wind Tunnel," *Proceedings of AIAA Ninth Aerodynamic Testing Conference*, June 1976, pp. 31-38.

[4]Kemp, W.B., Jr., "Transonic Assessment of Two-Dimensional Wind Tunnel Wall Interference Using Measured Wall Pressures," NASA Conference Publ. 2045, March 1978, pp. 473-486.

[5]Murman, E.M., "A Correction Method for Transonic Wind Tunnel Wall Interference," AIAA Paper 79-1533, July 1979.

[6]Mokry, M. and Ohman, L. H., "Application of the Fast Fourier Transform to Two-Dimensional Wind Tunnel Wall Interference," *Journal of Aircraft,* Vol. 17, June 1980, pp. 402-408.

[7]Murman, E.M., "Computation of Wall Effects in Ventilated Transonic Wind Tunnels," AIAA Paper 72-1007, Sept. 1972.

[8]Chan, Y.Y., "Perturbation Analysis of Transonic Wind Tunnel Wall Interference," *Journal of Aircraft,* Vol. 17, June 1980, pp. 409-411.

[9]Chan, Y.Y., "A Singular Perturbation Analysis of Two-Dimensional Wind Tunnel Interference," *Journal of Applied Mathematics and Physics,* Vol. 31, (ZAMP), 1980, pp. 1-15.

[10]Ashley, H. and Landhal, M.T., *Aerodynamics of Wings and Bodies,* Addison-Wesley, Reading, Mass., 1965, pp. 102, 129, 133.

[11]Adams, J., Swarztrauber, P., and Sweet, R., "FISHPAK, A Package of Fortran Subprograms for the Solution of Separable Elliptic Partial Differential Equations," NCAR, Boulder, Colo., June 1979.